Dual Regulation of Graphene Oxide Membrane by Crosslinker and Hydrophilic Promoter for Dye Separation

Ge Yang, Mengling Sun, Chunzheng Wang, Yanpeng Li, Yongming Chai, Hailing Guo, Svetlana Mintova

Dual Regulation of Graphene Oxide Membrane by Crosslinker and Hydrophilic Promoter for Dye Separation

Ge Yang[1], Mengling Sun[1], Chunzheng Wang[1], Yanpeng Li[2], Yongming Chai[1], Hailing Guo[1,*], Svetlana Mintova[1,3]

[1] State Key Laboratory of Heavy Oil Processing, College of Chemistry and Chemical Engineering, China University of Petroleum (East China) Qingdao 266555 (P.R. China).

[2] Advanced Chemical Engineering and Energy Materials Research Center, China University of Petroleum (East China) Qingdao 266555 (P.R. China).

[3] Laboratoire Catalyse et Spectrochimie (LCS), ENSICAEN, UNICAEN, CNRS, Normandie Université, 6 boulevard du Marechal Juin, 14050 Caen (France).

* Corresponding authors.

Email addresses: guohl@upc.edu.cn (Hailing. Guo)

Abstract

Graphene oxide (GO)-based membranes have shown considerable promise in the field of water treatment. However, the structural swelling of GO membranes in water has hindered their further development. A single regulatory approach seems difficult to simultaneously improve permeability, selectivity, and stability. In this study, we present a dual regulation strategy for GO membranes employing the 1,4-Diaminobutane crosslinker to prevent swelling and maintain an interlayer spacing of 1.34 nm, resulting in effective dye rejection, and employing the hydrophilic EMT-type zeolite promoter to improve the membrane's water permeability. The obtained NH_2-GO/10EMT composite membrane exhibited enhanced pure water flux (from 9.0 to 20.8 L/m^2·h·bar) and anionic dye rejection (from 87.2% to 97.6%) with promising structure stability (at least 20 h), while greatly improving the membrane's fouling resistance (the water recovery ratio increased from 46.5% to 86.2%). Our findings provide a straightforward and efficient approach to the development of high-performance GO membranes for selective water separation.

Keywords

Zeolite; Graphene oxide membrane; Hydrophilicity; Dye rejection; Anti-fouling

1 Introduction

The global freshwater resources crisis is being exacerbated by several factors, including population growth, climate change, groundwater depletion, and environmental pollution[1,2]. Membrane separation technology offers the advantages of high separation efficiency, facile operation, low energy consumption, and large water treatment capacity in wastewater treatment[3,4]. However, low fouling resistance is a significant issue faced by the mature polymer membranes used in wastewater treatment[5-7]. The inherent hydrophobicity possessed by polymer membranes renders them more prone to the adsorption of foulants[7]. Graphene oxide (GO) membranes with better hydrophilicity and surface roughness have the potential to be effective alternatives, due to their excellent permeability and sieving properties, especially the high membrane-forming ability[8-10]. Furthermore, the hydrophilicity of GO membranes confers advantageous anti-fouling performance, as the hydrophilic surface can inhibit the non-specific adsorption of pollutants such as proteins[7]. Yet, one of the primary drawbacks to using GO membranes in wastewater treatment is structural swelling. The edges of GO nanosheets are rich in active groups, which are readily hydrated, resulting in the interlayer channels expanding until the structure dissolves[11,12].

Numerous approaches have been employed to address the limitations of GO membranes, including chemical reduction[13-15], nanoparticle intercalation[16,17], and covalent cross-linking[18-20], to create stable GO membranes. However, the chemical reduction of GO membranes typically results in a decrease in *d*-spacing and

a sharp decline in total flux. The incorporation of nanoparticles via non-covalent bonding requires strong interactions (e.g. electrostatic interactions, hydrogen bonding interactions, coordination interactions, π-π interactions) between GO nanosheets and nanoparticles, which can be adversely affected by the working conditions of the membranes, such as polarity, and pH level[21]. Moreover, although the support effect of nanoparticles can improve the membrane's water flux, their insertion will disrupt the ordered stacking of GO nanosheets due to mismatched interlayer spacing and inorganic particle size. Alternatively, covalent crosslinkers can form strong bonds with GO nanosheets to build stable membranes, and the interlayer spacing can be adjusted by altering the molecular size of the crosslinkers[22,23]. However, the molecular size of the crosslinkers can impact the membranes' performance. Small-sized crosslinkers (e.g. ethylenediamine, urea, etc.) narrow the interlayer spacing and occupy channels, leading to low flux (usually below 5 $L/m^2 \cdot h \cdot bar$) [24,25]. While polymer crosslinkers (e.g. polydopamine, polyallylamine, etc.) cannot support interlayer channels with uniform d-spacing, thus affecting the membranes' size-sieving ability [21,26]. From the above research results, it can be seen that a single regulatory approach cannot simultaneously improve permeability, selectivity, and stability.

The concurrent implementation of both approaches, the "dual-regulation strategy", could be a viable option for enhancing structural stability and optimizing water treatment performance for GO membranes. For example, the researchers used nanoparticles as intercalating materials and polymer crosslinkers matching the

nanoparticles' size to ensure GO membrane structure stability. Table 1 summarizes several dual-regulated GO membranes. The large size particles (>100 nm) destroyed the ordered stacking of GO membranes. Although polymer crosslinkers could improve the stability of the GO membranes, they did not contribute to the construction of uniform interlayer channels. Thus, these dual-regulated GO membranes exhibited a low rejection of anionic dyes that require size-sieving property. However, the membranes demonstrated higher rejection for cationic dyes due to the adsorption of negatively charged GO membranes. Another case is that the structure of GO membrane is optimized by the synergetic coupling of ultra-small size nanoparticles and small-size crosslinkers. Kang's study made use of β-CD and monomer crosslinkers (TMC) in fabricating membranes with high selectivity for both anionic and cationic dyes[27]. Hence, effectively pairing intercalating materials and covalent crosslinkers based on their size and properties is a crucial aspect of executing the dual regulation strategy.

Table 1 Previous work about dual-regulated GO membranes

Membrane	Nanoparticle (size)	Crosslinker	Rejection of anionic dyes	Rejection of cationic dyes	Ref.
PDA/RGO /HKUST-1	HKUST-1 (ND)	PDA	CR 79.6%	MB 88.6%	[28]
PDA/RGO/UiO-66	UiO-66 (>200 nm)	PDA	CR 87.4%	MB 99.5%	[26]
PDA/RGO/MOFs& SiO_2-COOH	MOFs&SiO_2-COOH (900 nm)	PDA	ND	MB 99.4% MG 99%	[29]

PDA/RGO/HNTs	HNTs (~150 nm)	PDA	CR 99%	MB 99%	[30]
CNT/GO	CNT (15 nm)	MXDA	CR 98.7%	MB 94.1%	[31]
Ca/GO-SAx	Ca^{2+}	sodium alginate	CR 98.8%	MB 99.8%	[32]
GO/β-CD/TMC	β-CD (0.6 nm)	TMC	CR 99%	MB 99%	[27]

Note: PDA-polydopamine; TMC-trimesoyl chloride; MXDA-Meta-xylylenediamine; EDA-ethylenediamine

The use of zeolite materials in water treatment applications has gained attention due to their notable mechanical, thermal, and chemical stability are attractive for water treatment applications[33,34]. By adjusting the crystal morphology and the Si/Al ratio of the framework, hydrophilic zeolite nanocrystals can be synthesized, which can be employed as intercalated particles of GO membranes. EMT-type zeolite possesses hexagonal unit cells. In 2012, Mintova's group successfully synthesized EMT-type zeolite nanosheets with diameters below 20 nm and thicknesses below 10 nm without organic template[35]. These EMT-type zeolite nanosheets with a Si/Al ratio of only 1.14 exhibit strong hydrophilicity and hold promise as intercalation materials for GO membranes.

Here, we present a GO composite membrane that utilizes EMT-type zeolite nanosheets as a hydrophilic promoter and 1,4-Diaminobutane as a cross-linking agent (Scheme 1). The EMT-type nanosheets with a thickness of 6-7 nm, created hydrophilic regions within the GO membranes without disrupting the GO membranes' structure, allowing for an enhancement in water flux. On the other hand,

1,4-Diaminobutane contributed to the stabilization of the GO interlayer channels with big interlayer spacing (commonly termed as *d*-spacing) and confined EMT to the edge space of GO nanosheets by interlocking. The obtained composite GO/EMT membranes demonstrated enhanced hydrophilicity, and ordered interlayer channels, resulting in elevated water flux and superior rejection of anionic dyes, coupled with good anti-fouling performance.

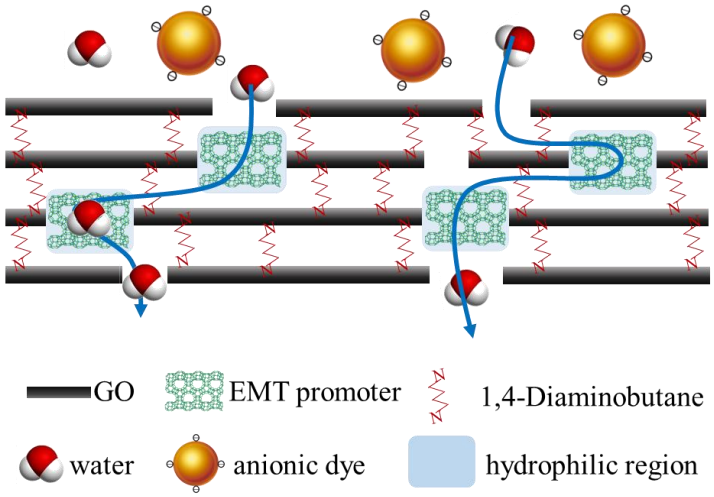

Scheme 1 Schematic diagram of the dual regulation strategy of EMT and 1,4-Diaminobutane on GO membranes

2 Materials and methods

2.1 Materials

The support Nylon membrane with a pore size of 0.2 μm was obtained from Whatman TM. Graphene oxide (thickness: 0.8-1.2 nm) was bought from XFNANO. Sodium aluminate (technical), hydrochloric acid (37 %), methyl orange dye (MO, 96%), congo red dye (CR, >98.0%), and reactive black 5 (RB, ≥50 %) were purchased from Aladdin Reagent Co. Ltd. Sodium silicate solution (Na_2O 10.6%, SiO_2 26.5%) was obtained from Sigma-Aldrich. The crosslinker, 1,4-Diaminobutane

(98%), was bought from Macklin. Sodium hydroxide (AR) was obtained from Sinopharm Chemical Reagent Co., Ltd. All the reagents were used in the experiments without any further purification.

2.2 Synthesis of EMT-type zeolite nanosheet

EMT-type zeolite nanosheet was synthesized based on our previous work[35]. 2.95 g NaOH and 14.70 g Na_2SiO_3 were added into 20.00 g deionized water to get the Si source. 11.52 g NaOH and 2.05 g $NaAlO_2$ were mixed with 25.00 g deionized water to obtain the Al source. The Al source was dropped into the Si source in an ice water bath to get the final synthetic solution with a molar ratio of 16.45 Na_2O: 1.0 Al_2O_3: 5.15 SiO_2: 240 H_2O. After aging for 30 min, the synthetic solution was hydrothermally crystallized at 35 ℃ for 24h. Finally, the treated solution was washed by centrifuged (12000 rpm, 30 min) until pH=7. The EMT-type zeolite nanosheets were obtained after freeze-drying for 36 h and was named EMT.

2.3 Preparation of NH_2-GO/EMT composite membranes

The preparation procedure is shown in Scheme 2. Firstly, 0.15 mg/mL GO solution was prepared by ultrasound dispersing GO powder in deionized water. NH_2-GO was obtained by adding 1.50 mL 1,4-Diaminobutane into 20 mL GO solution under stirring (600 rpm) and heating at 80 ℃ for 1.5 h. A certain amount (0 mg, 10 mg, and 20 mg) of EMT nanosheets was ultrasonically dispersed in deionized water (20 mL) for 1 h. Then, EMT was mixed with NH_2-GO evenly and the NH_2-GO/EMT composite membrane was obtained by vacuum filtration, named NH_2-GO/0EMT, NH_2-GO/10EMT, NH_2-GO/20EMT, respectively.

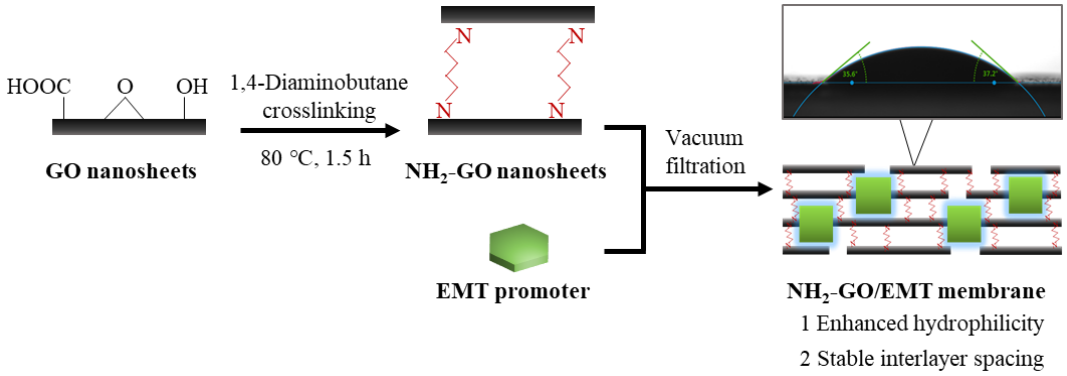

Scheme 2 Preparation of NH_2-GO/EMT composite membranes

2.4 Characterizations

The structures of EMT nanosheet and NH_2-GO/EMT composite membranes were measured by XRD (Bruker D8 Advance). The interlayer spacing (d) of membrane was calculated based on the Bragg equation: $2d\sin\theta=n\lambda$ (θ is the diffraction angle of membrane in XRD pattern, n stands for diffraction series 1, λ represents the 0.154056 nm wavelength of the Cu beam of XRD). The morphology of EMT nanosheet was observed by SEM (JEOL 7900F) and STEM (FEI Talos F200X 200kV). The surface and cross-sectional morphologies of NH_2-GO/EMT composite membranes were tested by SEM (JEOL 7900F) with EDS (Oxford Instruments X-MaxN). The membranes' surface properties were characterized with AMF (SHIMADZU, SMP-9700) and drop shape analyzer (KRUSS, DSA100). X-ray photoelectron spectroscopy of membranes was conducted on a ThermoFischer ESCALAB 250Xi X-ray Photoelectron Spectroscope with an Al K_α radiation source. The swelling degree (SD) was used to describe the structural stability of the membrane in solution, which was based on Jia's work[36] and was analyzed by the gravimetric method. Generally, the low SD means that the membrane has more stable structure. The membranes were weighed before (W_d) and after (W_w) soaking in

deionized water, and SD was calculated as SD=(W_w- W_d)/ Wd×100%.

2.5 Water flux and dye rejection performance

The water flux and dye rejection performance of the GO membrane and all crosslinked NH_2-GO/EMT membranes were studied using a dead-end unit (with a 3.14 cm^2 effective area) at 2 bar and 25 ℃. For each sample, 20 mL of the pure water or dye feed solutions with a concentration of 10 mg/L was used. The dye solutions include methyl orange dye (MO) with a molecular size of 1.13 nm×0.42 nm, congo red dye (CR) with a molecular size of 2.56 nm×0.73 nm, and reactive black 5 dye (RB) with a molecular size of 1.65 nm×1.65 nm, which are all anionic dyes. The long-term separation performance was measured by a cross-flow filter (with a 7.10 cm^2 effective area) at 2 bar and 25 ℃. The water flux J (L/m^2·h·bar) was measured by collecting the permeate water (V/L) through the membrane using an electronic balance and calculated using the following equation (1):

$$J = \frac{V}{A \times t \times P} \qquad (1)$$

Where A (m^2) is the effective membrane area, t (h) is the permeate time, and P (MPa) is the permeate pressure. UV-Vis spectrophotometer (UV mini 1240 Shimadzu) was also employed to measure the residual concentration of dye solution within the wavelength range of 200-700 nm based on the standard curve and the linear correlation coefficient was greater than 0.999. The rejection rate of organic dye molecules in an aqueous solution was calculated using the following equation (2):

$$R = \frac{C_{feed} - C_{permeate}}{C_{feed}} 100\% \qquad (2)$$

Where C_{feed} is the dye concentration in the feed solution, and $C_{permeate}$ is the dye

concentration in the permeate solution. All the water flux and dye separation performance results were obtained from at least three different GO membranes or composite membranes, and demonstrated using error bars.

2.6 Dye adsorption performance

In adsorption experiments, the MO dye solution with a concentration of 10 mg/L was used. GO/EMT composite membranes were placed in a 50 mL MO dye solution. The membrane samples were taken at intervals of 1h. The curve of time and ratio was drawn by measuring the absorbance of MO dye.

2.7 Anti-fouling property test

Bovine Serum Albumin (BSA) solution was used to test the membrane's anti-fouling property. Firstly, 10 mL of pure water was filtered through the membrane to obtain the pure water flux ($J_{w,\ 1}$). Secondly, 10 mL of BSA solution at a concentration of 100 ppm was filtered through the same membrane to obtain the BSA flux (J_{BSA}). Then, the fouled membrane was washed with water for 15 min to remove BSA. Then, the water flux ($J_{w,\ 2}$) of this membrane was measured again. The water flux recovery ratio (*FRR*) was calculated by the following equation (3):

$$FRR\ (\%) = \frac{J_{w,2}}{J_{w,1}} \times 100\% \qquad (3)$$

Fouling resistance ratios, including total fouling ratio (R_t), reversible fouling ratio (R_r), and irreversible fouling ratio (R_{ir}), were also applied to describe the anti-fouling performance of membranes. They were calculated according to the following equations (4-6):

$$R_t\ (\%) = (1 - \frac{J_{BSA}}{J_{w,1}}) \times 100\% \qquad (4)$$

$$R_r\ (\%) = \left(\frac{J_{w,2} - J_{BSA}}{J_{w,1}}\right) \times 100\% \qquad (5)$$

$$R_{ir}\ (\%) = \left(\frac{J_{w,1} - J_{w,2}}{J_{w,1}}\right) \times 100\% \qquad (6)$$

3 Results and discussion

3.1 Property of EMT nanosheets

As depicted in Figure 1(a), all primary characteristic Bragg peaks attributed to EMT-type zeolite were observed. Owing to the nanomaterial characteristic, the three peaks around 6° were combined into one broad peak, which was corroborated by the findings of previous literature[37]. The FT-IR spectrum also exhibited characteristic bands corresponding to EMT nanosheet, including the asymmetrical stretching vibration of the T-O-T band at 982 cm^{-1}, the double-6-ring (D6R) band at 567 cm^{-1}[38] (Figure 1(b)). These outcomes stated the successful synthesis of EMT-type zeolite. The EMT's morphology is presented in Figure 2, where the SEM image showed agglomerated nanosheets. However, independent nanosheets in a hexagonal shape could be observed in the TEM image, with a diameter of 20-30 nm and a thickness of 6-7 nm.

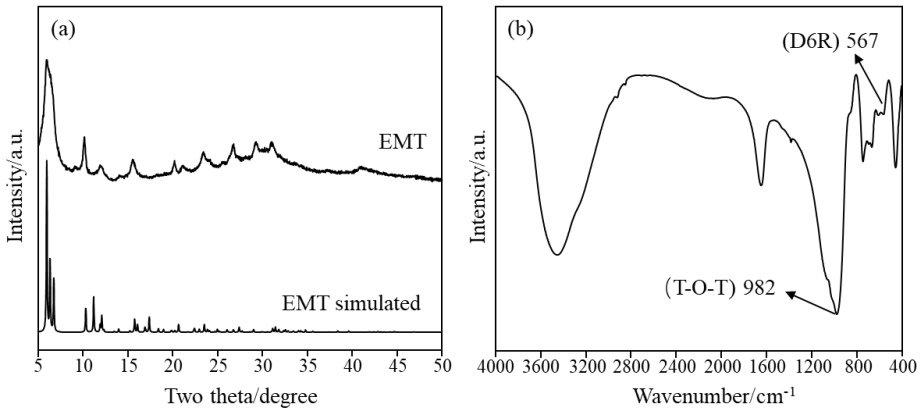

Figure 1 (a) XRD pattern and (b) FT-IR spectrum of EMT-type zeolite

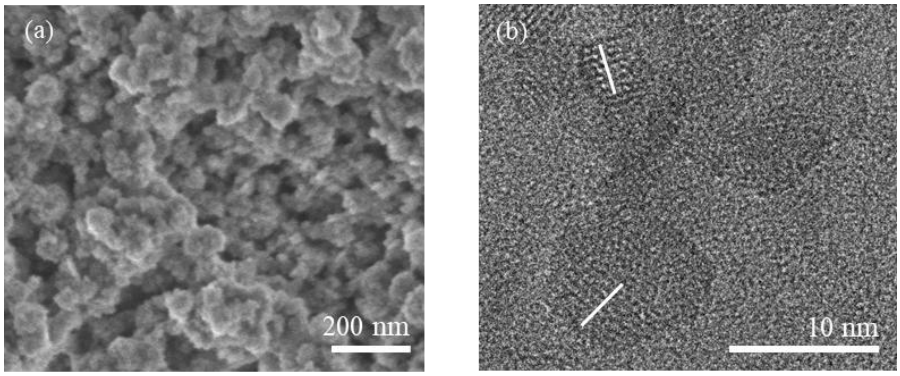

Figure 2 (a) SEM image and (b) TEM image of EMT-type zeolite nanosheet

3.2 Properties of NH_2-GO/EMT composite membranes

According to the XRD pattern, the dry GO membrane revealed a "*d*" spacing of 0.74 nm (11.9°), which aligns with previous studies[22,23,25]. With an SD of 58% (Table S1), the "*d*" spacing of the wet GO membrane rose to 1.02 nm. Upon cross-linking with 1,4-Diaminobutane, the layer spacing of the dry NH_2-GO/0EMT membrane was supported to 1.26 nm (7.0°), and its SD reduced to 15%, demonstrating the enhanced stability of NH_2-GO/0EMT membrane. Therefore, the layer spacing of the NH_2-GO/0EMT membrane was kept almost unchanged after contact with water (from 1.26 nm to 1.30 nm). All the composite membranes exhibited a bulge peak attributed to the EMT-type zeolite nanosheet. Due to the peak overlap of the EMT with the peak of the GO membrane, peak fitting analysis was conducted for composite membranes (Figure 3, right). The determination of the position of the three EMT peaks (the orange line) was carried out according to the (1,0,0), (0,0,2), and (1,0,1) planes of EMT[39], and the intensity ratio of these three peaks was consistent across all samples. In the case of the NH_2-GO/10EMT membrane, a narrow peak (the blue line) located at 6.6° was detected, indicating a relatively fixed layer spacing (d =1.34 nm) and resulting in an SD of only 28%.

However, a band with a larger FWHM (Full-Width Half-Maximum) instead of a narrow peak at 6.6° appeared in the NH_2-GO/20EMT membrane due to the destruction of interlayer spacing (the "*d*" spacing) by excessive zeolite nanosheets, thus also leading to a much higher SD of 54%. Hence, The NH_2-GO/10EMT composite membrane demonstrated regular layer spacing, thanks to the dual regulation of EMT nanosheets with 1,4-Diaminobutane crosslinkers. Additionally, the "*d*" spacing is smaller than the particle size of EMT nanosheets, signifying a presence within the free space between GO nanosheets.

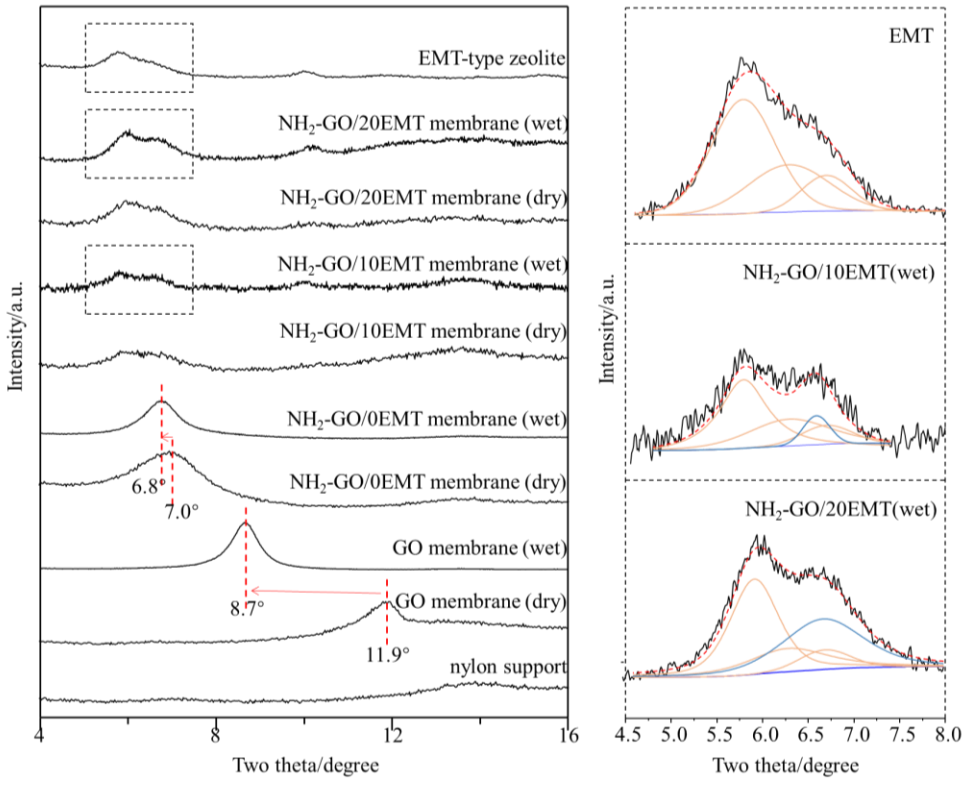

Figure 3 Left: XRD patterns of samples; Right: peak fitting of XRD patterns of EMT, NH_2-GO/10EMT membrane (wet) and NH_2-GO/20EMT membrane (wet)

Various functional groups can be identified in GO's FT-IR spectrum (Figure 4(a)), including C=O groups at 1724 cm^{-1}, -OH groups at 1399 cm^{-1}, and C-O-C groups at 1074 cm^{-1}[40,41]. After cross-linking with 1,4-Diaminobutane (Figure 4(b)), the C=O

band of the NH_2-GO/20EMT sample disappeared, while the intensity of the –OH band reduced significantly, indicating that 1,4-Diaminobutane reduced GO. Two new bands at 1568 cm^{-1} and 1475 cm^{-1}, attributed to –NH and C-N appeared, implying that 1,4-Diaminobutane reacted with GO's functional groups (specifically, C-OH). Similar changes of characteristic bands of GO after cross-linking with diamine can also be seen in the spectra of NH_2-GO/10EMT and NH_2-GO/20EMT composite membranes, and the band belonging to the EMT's skeleton T-O-T appeared at 983 cm^{-1}, which stated EMT promoter successfully introduced into the GO-based composite membranes.

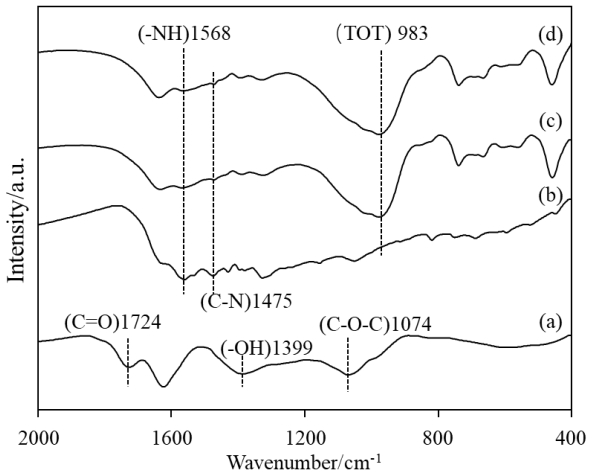

Figure 4 FT-IR spectra of (a) GO, (b) NH_2-GO/0EMT, (c) NH_2-GO/10EMT, and (d) NH_2-GO/20EMT

The C 1s peaks of GO showed peak binding energies of 284.8 eV, 286.1 eV, 286.8 eV, 288.1 eV, and 289.0 eV which correspond to C-C, C-O, C=O, and O-C=O, respectively(Figure 5a)[22,42,43]. However, the oxygen-containing groups were lost after the cross-linking reaction (Figure 5(b-d)). The intensity of C-O and O-C=O peaks of crosslinked GO membranes decreased significantly, but a new peak attributed to a C-N bond appeared[22]. By combining the XPS and FT-IR results, it

can be seen that the cross-linking reaction is mainly conducted by amidation.

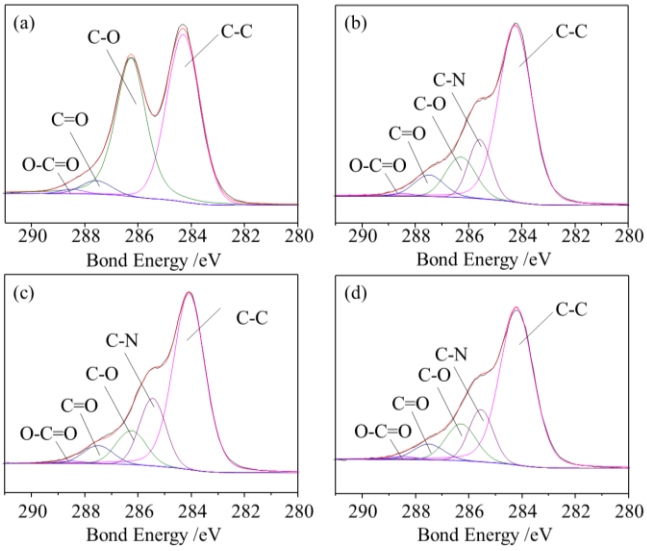

Figure 5 XPS elemental analysis of GO membrane and crosslinked GO membrane in the C1s region: (a) GO, (b) NH_2-GO/0EMT, (c) NH_2-GO/10EMT, and (d) NH_2-GO/20EMT

The cross-sectional SEM images indicated that the pure GO membrane with a thickness of 0.8 μm, displayed a lamellar morphology (Figure 6(a)). Following chemical cross-linking, the membrane's thickness increased to 1.0 μm, while still retaining its lamellar structure. The thickness of the composite membranes further increased to 2.5 μm and 3.0 μm after doping with 10.0 mg and 20.0 mg EMT nanosheets. It was observed that the cross-sectional structure of the NH_2-GO/10EMT membrane was denser, whereas that of the NH_2-GO/20EMT membrane was relatively rough, due to excessive EMT nanosheets influencing the membrane's structure.

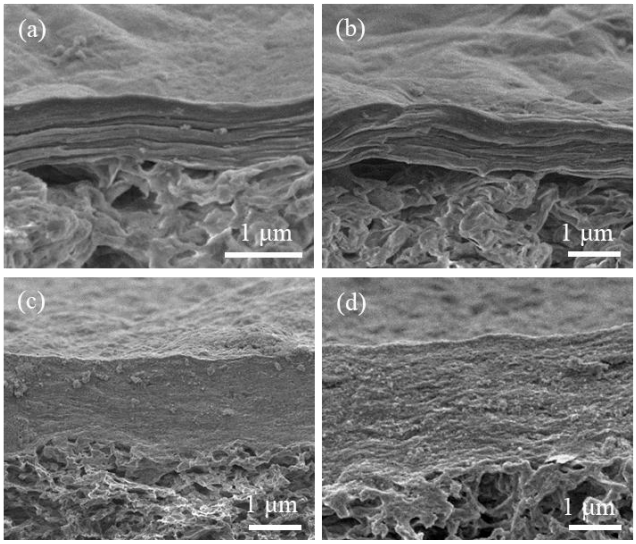

Figure 6 Cross-sectional SEM images of (a) GO membrane, (b) NH_2-GO/0EMT membrane, (c) NH_2-GO/10EMT membrane, and (d) NH_2-GO/20EMT membrane

The surface of the GO membrane showed a characteristic wrinkle morphology[9,44], with no apparent morphological changes observed after cross-linking (Figure 7 a,b). However, the elemental analysis indicated the presence of N element belonging to the diamine cross-linking agent (Figure 7(b)). The incorporation of EMT nanosheets resulted in the appearance of a granular morphology on the membranes' surface, with the presence of Al element attributed to EMT-type zeolite (Figure 7(c-d)). Additionally, the surface roughness of all membranes increased with the increased loading of cross-linking agents and zeolite promoters (Figure 8), which was consistent with the surface SEM images.

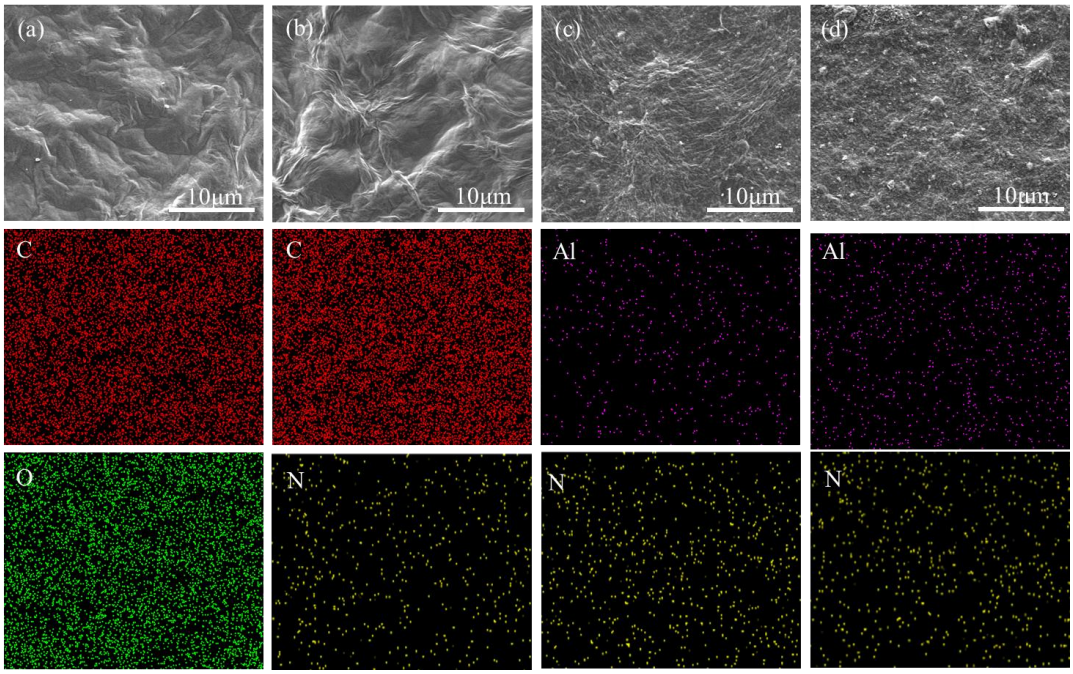

Figure 7 SEM images with EDS of the surface for (a) GO membrane, (b) NH_2-GO/0EMT membrane, (c) NH_2-GO/10EMT membrane, and (d) NH_2-GO/20EMT membrane

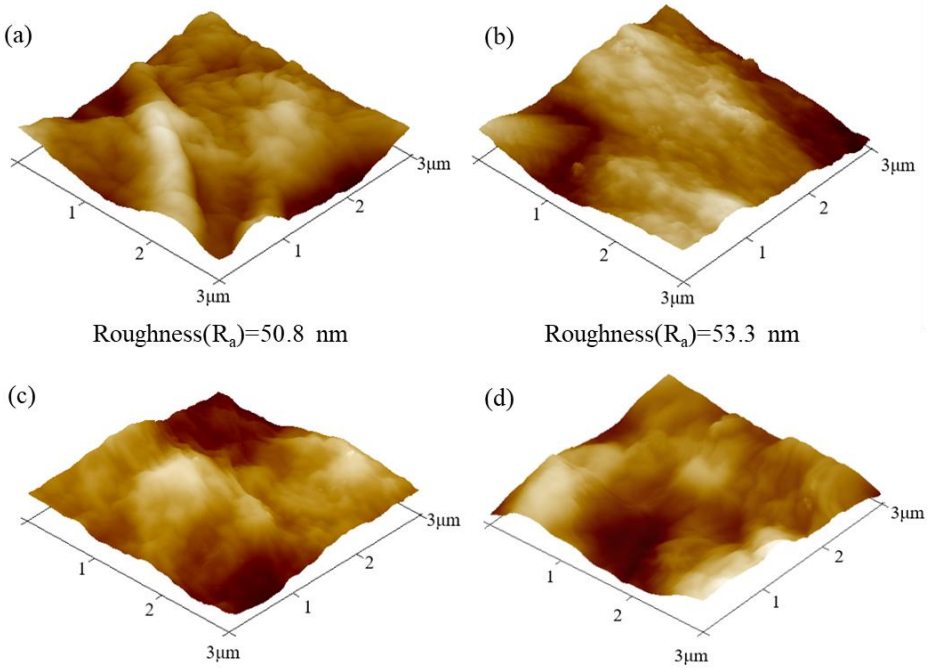

Figure 8 Surface roughness of (a) GO membrane, (b) NH_2-GO/0EMT membrane, (c) NH_2-GO/10EMT membrane, and (d) NH_2-GO/20EMT membrane

The original GO membrane had a common water contact angle of 53.4 º[22,23]. The water contact angle of NH_2-GO/0EMT membrane after cross-linked with 1,4-Diaminobutane increased to 58.1 º (Figure 9). The higher water contact angle

resulted from the introduction of hydrophobic alkyl groups and the loss of GO's oxygen-containing polar groups. However, the contact angle was reduced with an increase of EMT (33.5 º to 31.1 º), as EMT promoters improved the hydrophilic property of GO-based composite membranes (Figure S1), which would potentially enhance the membrane's water permeability.

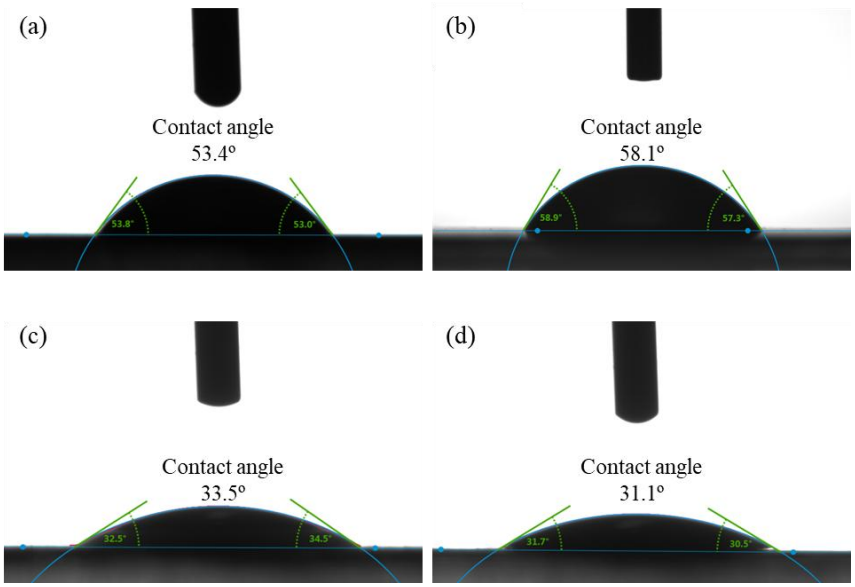

Figure 9 Water contact angle of (a) GO membrane, (b) NH_2-GO/0EMT membrane, (c) NH_2-GO/10EMT membrane, and (d) NH_2-GO/20EMT membrane

The pure GO membrane demonstrated a water flux of 9.0 L/m^2·h·bar, while the cross-linked NH_2-GO/0EMT membrane exhibited a decreased water flux of 4.3 L/m^2·h·bar, ascribed to the enhanced hydrophobicity (Figure 10). The water flux of the NH_2-GO/10EMT and NH_2-GO/20EMT composite membranes enhanced to 20.8 L/m^2·h·bar and 28.3 L/m^2·h·bar respectively, confirming the optimized effect of EMT promoters on membrane permeability (Figure 10).

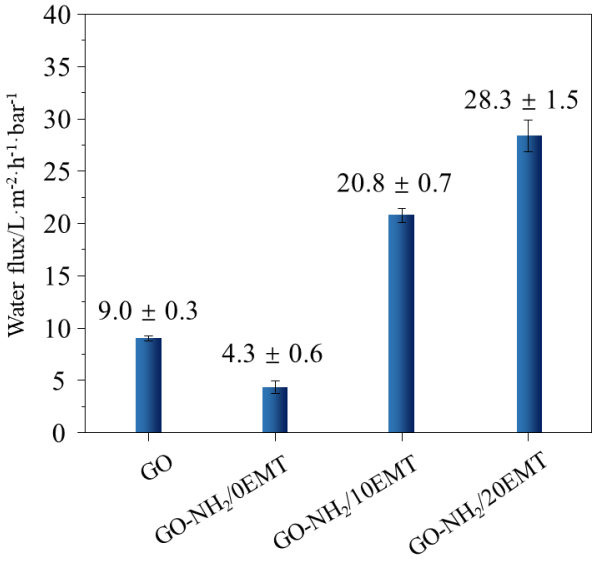

Figure 10 Water flux of GO membrane and crosslinked GO membranes

3.3 Dye separation performance

To evaluate dye separation performance, anionic methyl orange (MO) with a molecular size of 1.2~1.45 nm[45,46] was used (Figure 11). The GO membrane exhibited a flux of 5.9 L/m^2·h·bar and an 87.0 % rejection. The NH_2-GO/0EMT membrane with a more stable layer spacing, exhibited an increased rejection of 96.8%, while the low hydrophilicity of NH_2-GO/0EMT led to a reduced flux to 3.0 L/m^2·h·bar. EMT promoter significantly increased the MO flux of the composite membranes. The NH_2-GO/10EMT membrane achieved an enhanced MO flux of 11.2 L/m^2·h·bar and a higher rejection of 98.2%, highlighting the advantages of the dual regulation strategy in this work. With a further increase of EMT promoters, the MO flux of NH_2-GO/20EMT membrane increased to 18.5 L/m^2·h·bar, the rejection fell to 79.0%. This can be attributed to the excessive promoters that caused a disruption of the ordered structure of the NH_2-GO/20EMT membrane and reduced the size-sieving ability.

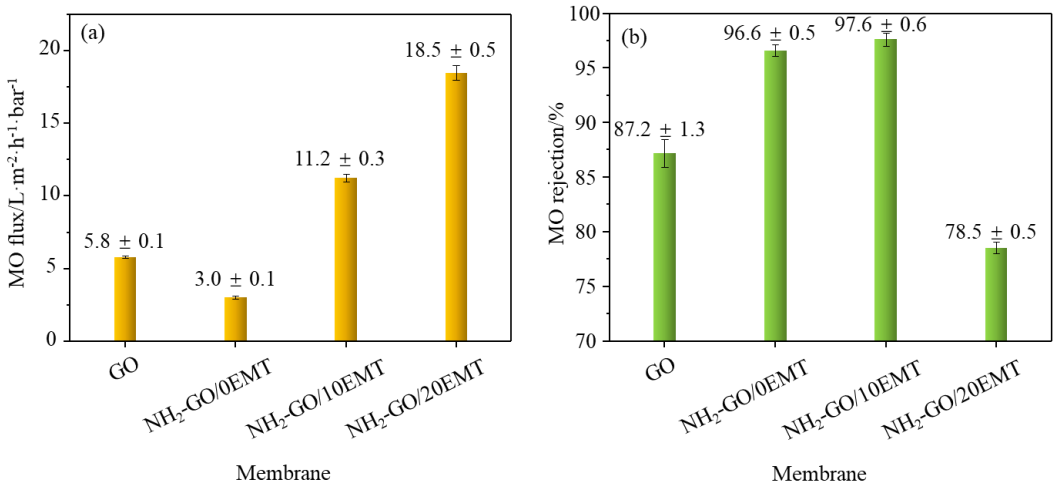

Figure 11 MO separation performance of membranes: (a) water flux and (b) MO rejection

As shown in Figure S2, the NH_2-GO/10EMT membrane possessed minimal adsorption capability for anionic MO, suggesting that the membrane's dye separation performance primarily relied on the interception of MO molecules. Based on the XRD analysis, the layer spacing of the NH_2-GO/10EMT membrane is about 1.34 nm, a dimension comparable to that of the methyl orange molecule. This may result in inadequate retention of certain dye molecules. Therefore, congo red (CR) and reactive black 5 (RB) dyes were employed as substitutes, due to their comparatively larger molecular size[46], as illustrated in Figure 12. The findings indicated that the NH_2-GO/10EMT membrane successfully achieved a higher rejection rate of over 99.5%, verifying the size interception ability of the NH_2-GO/10EMT composite membrane. As depicted in Figure S3, the high CR rejection and water flux of 13-14 $L/m^2 \cdot h \cdot bar$ of NH_2-GO/10EMT membrane within 20 h confirmed the structural stability and sieving property of the membrane.

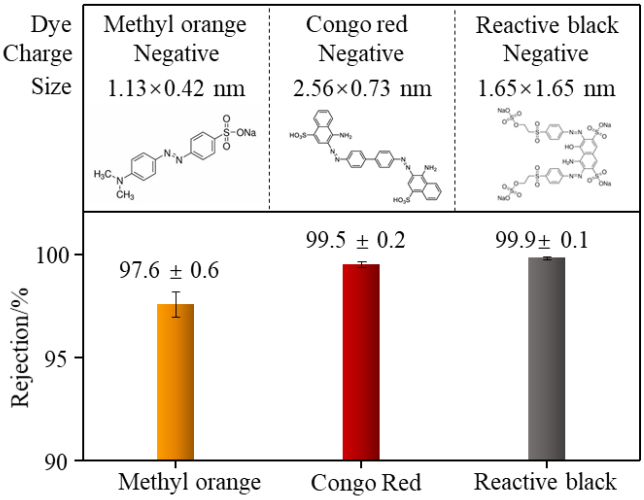

Figure 12 Dye rejection performance of NH_2-GO/10EMT membrane for different dyes

3.4 Anti-fouling performance

The anti-fouling performance of the membranes was evaluated by assessing the filtration of a 100 ppm Bovine Serum Albumin (BSA) solution. As shown in Figure 13, the water flux demonstrated a marked decrease during the BSA solution filtration. Unfortunately, due to the unstable structure of the GO membrane, the membrane structure was damaged during the cleaning process after contamination, so the membrane could not be reused (Figure 13 a). However, the cross-linking of 1,4-Diaminobutane improved the structural integrity of the crosslinked NH_2-GO/0EMT and NH_2-GO/10EMT membranes, rendering the crosslinked membranes amenable to washing and restoration of water flux. The recovered water flux of the NH_2-GO/10EMT membrane remained around 17.0 $L/m^2 \cdot h \cdot bar$, indicating high anti-fouling performance.

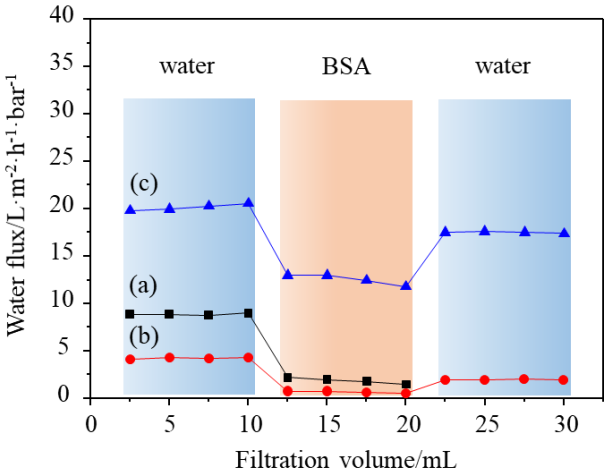

Figure 13 Anti-fouling performance of (a) GO, (b) NH_2-GO/0EMT and (c) NH_2-GO/10EMT membranes

The membrane's anti-fouling performance was explored by comprising water flux recovery ratios and fouling resistance ratios, as shown in Figure 14. The NH_2-GO/10EMT membrane exhibited a higher *FRR* (86.2%) than the NH_2-GO/0EMT membrane (46.5%), indicating that the increase of hydrophilicity could improve the anti-fouling property. The hydrophilic surface could preferentially adsorb water molecules, thus preventing the adsorption of other fouling agents[47,48]. Moreover, the EMT-modified crosslinked membrane (NH_2-GO/10EMT) had a lower R_t and a higher R_r than the NH_2-GO/0EMT membrane. This may be due to the increased hydrophilicity of the membrane surface and the presence of hydrophilic free spaces within the membrane, which promoted the diffusion of water and reduced deposition of BSA in the membrane's channel. Therefore, the EMT promoter has significantly improved the water flux and anti-fouling performance of crosslinked membranes.

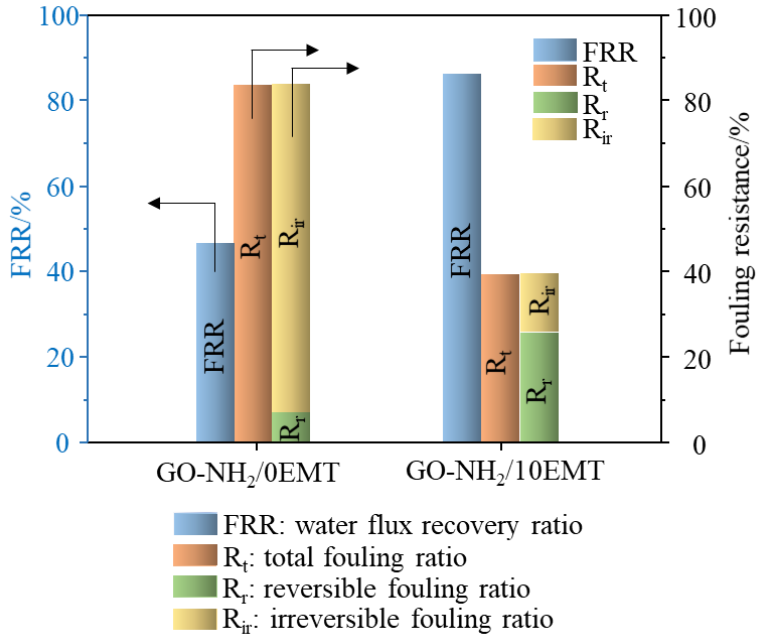

Figure 14 Water flux recovery ratios and fouling resistance ratios of GO membrane, NH_2-GO/0EMT and NH_2-GO/10EMT membranes

3.5 The promotion of dual regulation strategy on membrane's water flux

NH_2-GO/10EMT membrane was compared with other crosslinked GO membranes using diamine crosslinkers (Table 2). Firstly, the incorporation of EMT nanosheets resulted in a noticeable decrease of the contact angle of the GO/EMT composite membrane to 33.5°, indicating an enhancement of the membrane hydrophilicity in contrast to other crosslinked GO membranes. Secondly, the utilization of 1,4-Diaminobutane crosslinker over other cross-linking agents resulted in the extension of the interlayer spacing of the composite membrane up to 1.34 nm, thus also promoting the diffusion of water molecules. Therefore, this dual-regulated GO membranes demonstrated an enhanced water flux.

Table 2 Comparison of different crosslinked GO membranes

Membrane	Crosslinker	Contact angle/°	*d* /nm	Pure water flux/ $L/m^2 \cdot h \cdot bar$	Ref
GO-EDA/CA	ethylenediamine	24.4	0.93	1.3	[49]
GO-BDA/CA	butylenediamine	26.6	0.99	2.4	
GO-PPD/CA	p-phenylenediamine	80.6	1.09	0.3	
GO-UR/CA	urea	64.7	0.85	~9	[25]
GO-EDA/CA	Ethylenediamine	94.8	0.89	~7	
GO-PPD 1bL	p-phenylenediamine	53.2	/	6.2	[5]
GO-PPD 5bL	p-phenylenediamine	59.7	/	1.8	
A2-GO	1,2-Diaminoethane	44.2	0.85	~3 (45℃)	[23]
A3-GO	1,3-Diaminopropane	51.4	0.95	~3 (45℃)	
A4-GO	1,4-Diaminobutane	54.9	1.06	~4 (45℃)	
BPPO/EDA/GO	ethylenediamine	/	/	4.1	[50]
PDA-GO/EDA	ethylenediamine	53.4	1.13	30.8	[51]
PDA-GO/beta-CD-EDA	beta-CD-EDA	70.53	0.97	34.0	
GO&EDA	ethylenediamine	/	/	17.9	[52]
GO&EDA_HPEI 60K	ethylenediamine	/	/	5.01	
NH_2-GO/10EMT	1,4-Diaminobutane with EMT promoter	33.5	1.34	20.8	This work

4 Conclusions

In this work, the combined use of a 1,4-Diaminobutane crosslinker and a hydrophilic EMT promoter yielded a synergistic effect on the dual regulation of GO membranes. The 1,4-Diaminobutane crosslinker stabilized the composite membrane structure and limited the layer spacing to 1.34 nm. The EMT nanosheets were locked in the free space of the composite membranes to construct hydrophilic regions. As a result, the NH_2-GO/10EMT composite membrane exhibited significant improvement in its hydrophilicity, with the pure water flux increasing from 4.3 $L/m^2 \cdot h \cdot bar$ to 21.1 $L/m^2 \cdot h \cdot bar$. The molecular size of the anionic dyes affected the rejection, as methyl

orange with a smaller molecular size had a rejection of 96.8%, while congo red and reactive black, which have larger molecular sizes, had a rejection of more than 99%. Furthermore, our investigation showed a significant improvement in the fouling profile of the NH_2-GO/10EMT membrane, with higher water flux recovery ratio and lower fouling ratio. To conclude, the NH_2-GO/10EMT composite membrane, prepared by dual regulation strategy, proved highly efficient in dye separation and displayed good anti-fouling property. This work presents a feasible optimization strategy to enhance the hydrophilicity of GO crosslinked membranes on the premise of ensuring their ordered lamellar structure.

Declaration of Competing Interest

The authors declared that they have no known competing financial interests or personal relationships that could have appeared to influence the work reported in this paper.

Acknowledgements

This work is supported by National Key Research and Development Program of China of Ministry of Science and Technology (2022YFE0116000), National Natural Science Foundation of China (Grant No. 22175200, No. 21975285), the Fundamental Research Funds for the Central Universities (No. 21CX06024A), Qingdao Postdoctoral Research Project (No. qdyy20210005), and Innovation Fund of Science and Technology Project of Fujian Province (2022C0021).

References

[1] Z. Li, X. Xu, X. Sheng, P. Lin, J. Tang, L. Pan, Y.V. Kaneti, T. Yang, Y. Yamauchi, Solar-powered sustainable water production: State-of-the-art technologies for

sunlight-energy-water nexus, ACS Nano 15 (8) (2021) 12535-12566. https://doi.org/10.1021/acsnano.1c01590.

[2] M. Salehi, Global water shortage and potable water safety; Today's concern and tomorrow's crisis, Environ. Int. 158 (2022) 106936. https://doi.org/10.1016/j.envint.2021.106936.

[3] J. Dasgupta, J. Sikder, S. Chakraborty, S. Curcio, E. Drioli, Remediation of textile effluents by membrane based treatment techniques: A state of the art review, J. Environ. Manage. 147 (2015) 55-72. https://doi.org/10.1016/j.jenvman.2014.08.008.

[4] D. Sholl, R. Lively, Seven chemical separations to change the world, Nature 532 (7600) (2016) 435-437. https://doi.org/10.1038/532435a.

[5] V. Kandjou, A.M. Perez-Mas, B. Acevedo, M. Hernaez, A.G. Mayes, S. Melendi-Espina, Enhanced covalent p-phenylenediamine crosslinked graphene oxide membranes: Towards superior contaminant removal from wastewaters and improved membrane reusability, J. Hazard. Mater. 380 (2019) 120840. https://doi.org/10.1016/j.jhazmat.2019.120840.

[6] X. Lu, M. Elimelech, Fabrication of desalination membranes by interfacial polymerization: history, current efforts, and future directions, Chem. Soc. Rev. 5 (11) (2021) 629-637. https://doi.org/10.1039/d0cs00502a.

[7] R. Zhang, Y. Liu, M. He, Y. Su, X. Zhao, M. Elimelech, Z. Jiang, Antifouling membranes for sustainable water purification: strategies and mechanisms, Chem. Soc. Rev. 45 (21) (2016) 5888-5924. https://doi.org/10.1039/c5cs00579e.

[8] J. Abraham, K.S. Vasu, C.D. Williams, K. Gopinadhan, Y. Su, C.T. Cherian, J. Dix, E. Prestat, S.J. Haigh, I.V. Grigorieva, P. Carbone, A.K. Geim, R.R. Nair, Tunable sieving of ions using graphene oxide membranes, Nat. Nanotechnol. 12 (6) (2017) 546-550.

https://doi.org/10.1038/nnano.2017.21.

[9] H. Huang, Z. Song, N. Wei, L. Shi, Y. Mao, Y. Ying, L. Sun, Z. Xu, X. Peng, Ultrafast viscous water flow through nanostrand-channelled graphene oxide membranes, Nat. Commun. 4 (1) (2013) 2979. https://doi.org/10.1038/ncomms3979.

[10] M. Sun, J. Li, Graphene oxide membranes: functional structures, preparation and environmental applications, Nano Today 20 (2018) 121-137. https://doi.org/10.1016/j.nantod.2018.04.007.

[11] Y. An, X. Gao, W. Jiang, J. Han, Y. Ye, T. Chen, R. Ren, J. Zhang, B. Liang, Z. Li, A. Wang, N. Ren, A critical review on graphene oxide membrane for industrial wastewater treatment, Environ. Res. 223 (2023) 115409. https://doi.org/10.1016/j.envres.2023.115409.

[12] J. Wang, H. Zhou, S. Li, L. Wang, Selective ion transport in two- dimensional lamellar nanochannel membranes, Angew. Chem. Int. Ed. 62 (19) (2023) e202218321. https://doi.org/10.1002/anie.202218321.

[13] A. Mohammadi, M.R. Daymond, A. Docoslis, New insights into the structure and chemical reduction of graphene oxide membranes for use in isotopic water separations, J. Membrane Sci. 659 (2022) 120785. https://doi.org/10.1016/j.memsci.2022.120785.

[14] Y. Li, S. Yuan, Y. Xia, W. Zhao, C.D. Easton, C. Selomulya, X. Zhang, Mild annealing reduced graphene oxide membrane for nanofiltration, J. Membrane Sci. 601 (2020) 117900. https://doi.org/10.1016/j.memsci.2020.117900.

[15] X. Fan, C. Cai, J. Gao, X. Han, J. Li, Hydrothermal reduced graphene oxide membranes for dyes removing, Sep. Purif. Technol. 241 (2020) 116730. https://doi.org/10.1016/j.seppur.2020.116730.

[16] L. Chen, G. Shi, J. Shen, B. Peng, B. Zhang, Y. Wang, F. Bian, J. Wang, D. Li, Z. Qian, G. Xu, G. Liu, J. Zeng, L. Zhang, Y. Yang, G. Zhou, M. Wu, W. Jin, J. Li, H. Fang, Ion sieving in graphene oxide membranes via cationic control of interlayer spacing, Nature 550 (7676) (2017) 380-383. https://doi.org/10.1038/nature24044.

[17] Y. Ying, D. Liu, W. Zhang, J. Ma, H. Huang, Q. Yang, C. Zhong, High-flux graphene oxide membranes intercalated by metal–organic framework with highly selective separation of aqueous organic solution, ACS Appl. Mater. Inter. 9 (2) (2017) 1710-1718. https://doi.org/10.1021/acsami.6b14371.

[18] R.P. Pandey, P. Kallem, H.M. Hegab, P.A. Rasheed, F. Banat, S.W. Hasan, Cross-linked laminar graphene oxide membranes for wastewater treatment and desalination: A review, J. Environ. Manage. 317 (2022) 115367. https://doi.org/10.1016/j.jenvman.2022.115367.

[19] A. Alkhouzaam, H. Qiblawey, Functional GO-based membranes for water treatment and desalination: fabrication methods, performance and advantages. A review, Chemosphere 274 (2021) 129853. https://doi.org/10.1016/j.chemosphere.2021.129853.

[20] S. Sharif, K.S. Ahmad, F. Rehman, Z. Bhatti, K.H. Thebo, Two-dimensional graphene oxide based membranes for ionic and molecular separation: current status and challenges, J. Environ. Chem. Eng. 9 (4) (2021) 105605. https://doi.org/10.1016/j.jece.2021.105605.

[21] X. Lv, R. Xie, J. Ji, Z. Liu, X. Wen, L. Liu, J. Hu, X. Ju, W. Wang, L. Chu, A novel strategy to fabricate cation-cross-linked graphene oxide membrane with high aqueous stability and high separation performance, ACS Appl. Mater. Inter. 12 (50) (2020) 56269-56280. https://doi.org/10.1021/acsami.0c15178.

[22] H. Ju, J. Duan, H. Lu, W. Xu, Cross-linking with diamine monomers to prepare graphene

oxide composite membranes with varying *d*-spacing for enhanced desalination properties, Front. Chem. 9 (2021) 779304. https://doi.org/10.3389/fchem.2021.779304.

[23] Y. Qian, X. Zhang, C. Liu, C. Zhou, A. Huang, Tuning interlayer spacing of graphene oxide membranes with enhanced desalination performance, Desalination 460 (2019) 56-63. https://doi.org/10.1016/j.desal.2019.03.009.

[24] K. Guan, K. Ushio, K. Nakagawa, T. Shintani, T. Yoshioka, A. Matsuoka, E. Kamio, W. Jin, H. Matsuyama, Integration of thin film composite graphene oxide membranes for solvent resistant nanofiltration, J. Membrane Sci. 660 (2022) 120861. https://doi.org/10.1016/j.memsci.2022.120861.

[25] Y. Zhang, K. Su, Z. Li, Graphene oxide composite membranes cross-linked with urea for enhanced desalting properties, J. Membrane Sci. 563 (2018) 718-725. https://doi.org/10.1016/j.memsci.2018.06.037.

[26] Y. Liu, D. Gan, M. Chen, L. Ma, B. Yang, L. Li, M. Zhu, W. Tu, Bioinspired dopamine modulating graphene oxide nanocomposite membrane interposed by super-hydrophilic UiO-66 with enhanced water permeability, Sep. Purif. Technol. 253 (2020) 117552. https://doi.org/10.1016/j.seppur.2020.117552.

[27] J. Pang, X. Cui, Y. Feng, Z. Guo, G. Kong, L. Yu, C. Zhang, R. Wang, Z. Kang, D. Sun, Fabrication of graphene oxide membrane with multiple “plug-ins” for efficient dye nanofiltration, Sep. Purif. Technol. 278 (2021) 119504. https://doi.org/10.1016/j.seppur.2021.119504.

[28] Y. Liu, M. Zhu, M. Chen, L. Ma, B. Yang, L. Li, W. Tu, A polydopamine-modified reduced graphene oxide (RGO)/MOFs nanocomposite with fast rejection capacity for organic dye,

Chem. Eng. J. 359 (2019) 47-57. https://doi.org/10.1016/j.cej.2018.11.105.

[29] Y. Liu, Z. Huang, W. He, M. Chen, W. Tu, M. Zhu, D. Gan, S. Liu, Multifunctional stable PDA/RGO/MOFs&SiO_2-COOH membrane with excellent flux and anti-fouling performance for the separation of organic dye and oil/water, Surf. Interfaces 33 (2022) 102183. https://doi.org/10.1016/j.surfin.2022.102183.

[30] Y. Liu, W. Tu, M. Chen, L. Ma, B. Yang, Q. Liang, Y. Chen, A mussel-induced method to fabricate reduced graphene oxide/halloysite nanotubes membranes for multifunctional applications in water purification and oil/water separation, Chem. Eng. J. 336 (2018) 263-277. https://doi.org/10.1016/j.cej.2017.12.043.

[31] L. Huang, Z. Li, Y. Luo, N. Zhang, W. Qi, E. Jiang, J. Bao, X. Zhang, W. Zheng, B. An, G. He, Low-pressure loose GO composite membrane intercalated by CNT for effective dye/salt separation, Sep. Purif. Technol. 256 (2021) 117839. https://doi.org/10.1016/j.seppur.2020.117839.

[32] J. Yu, Y. Wang, Y. He, Y. Gao, R. Hou, J. Ma, L. Zhang, X. Guo, L. Chen, Calcium ion-sodium alginate double cross-linked graphene oxide nanofiltration membrane with enhanced stability for efficient separation of dyes, Sep. Purif. Technol. 276 (2021) 119348. https://doi.org/10.1016/j.seppur.2021.119348.

[33] L. Wang, J. Yang, J. Wang, W. Raza, G. Liu, J. Lu, Y. Zhang, Microwave synthesis of NaA zeolite membranes on coarse macroporous α-Al_2O_3 tubes for desalination, Micropor. Mesopor. Mat. 306 (2020) 110360. https://doi.org/10.1016/j.micromeso.2020.110360.

[34] W. Raza, J. Wang, J. Yang, T. Tsuru, Progress in pervaporation membranes for dehydration of acetic acid, Sep. Purif. Technol. 262 (2021) 118338.

https://doi.org/10.1016/j.seppur.2021.118338.

[35] E.P. Ng, D. Chateigner, T. Bein, V. Valtchev, S. Mintova, Capturing ultrasmall EMT zeolite from template-free systems, Science 335 (6064) (2012) 70-73. https://doi.org/10.1126/science.1214798.

[36] Z. Jia, Y. Wang, W. Shi, J. Wang, Diamines cross-linked graphene oxide free-standing membranes for ion dialysis separation, J. Membrane Sci. 520 (2016) 139-144. https://doi.org/10.1016/j.memsci.2016.07.042.

[37] E. Ng, J. Goupil, A. Vicente, C. Fernandez, R. Retoux, V. Valtchev, S. Mintova, Nucleation and crystal growth features of EMT-type zeolite synthesized from an organic-template-free system, Chem. Mater. 24 (24) (2012) 4758-4765. https://doi.org/10.1021/cm3035455.

[38] S. Xia, Y. Chen, H. Xu, D. Lv, J. Yu, P. Wang, Synthesis EMT-type zeolite by microwave and hydrothermal heating, Micropor. Mesopor. Mat. 278 (2019) 54-63. https://doi.org/https://doi.org/10.1016/j.micromeso.2018.11.012.

[39] A. Nearchou, P.R. Raithby, A. Sartbaeva, Systematic approaches towards template-free synthesis of EMT-type zeolites, Micropor. Mesopor. Mat. 255 (2018) 261-270. https://doi.org/10.1016/j.micromeso.2017.08.036.

[40] G. Zhao, J. Li, X. Ren, C. Chen, X. Wang, Few-layered graphene oxide nanosheets as superior sorbents for heavy metal ion pollution management, Environ. Sci. Technol. 45 (24) (2011) 10454-10462. https://doi.org/10.1021/es203439v.

[41] J. Shen, B. Yan, M. Shi, H. Ma, N. Li, M. Ye, One step hydrothermal synthesis of TiO_2-reduced graphene oxide sheets, Journal of materials chemistry 21 (10) (2011) 3415. https://doi.org/10.1039/c0jm03542d.

[42] R. Al-Gaashani, A. Najjar, Y. Zakaria, S. Mansour, M.A. Atieh, XPS and structural studies of high quality graphene oxide and reduced graphene oxide prepared by different chemical oxidation methods, Ceram. Int. 45 (11) (2019) 14439-14448. https://doi.org/10.1016/j.ceramint.2019.04.165.

[43] C. Jiao, J. Xiong, J. Tao, S. Xu, D. Zhang, H. Lin, Y. Chen, Sodium alginate/graphene oxide aerogel with enhanced strength–toughness and its heavy metal adsorption study, Int. J. Biol. Macromol. 83 (2016) 133-141. https://doi.org/10.1016/j.ijbiomac.2015.11.061.

[44] H.W. Kim, H.W. Yoon, S. Yoon, B.M. Yoo, B.K. Ahn, Y.H. Cho, H.J. Shin, H. Yang, U. Paik, S. Kwon, J. Choi, H.B. Park, Selective gas transport through few-layered graphene and graphene oxide membranes, Science 342 (6154) (2013) 91-95. https://doi.org/10.1126/science.1236098.

[45] S. Ko, T. Yamaguchi, F. Salles, J. Oh, Systematic utilization of layered double hydroxide nanosheets for effective removal of methyl orange from an aqueous system by π-π stacking-induced nanoconfinement, J. Environ. Manage. 277 (2021) 111455. https://doi.org/10.1016/j.jenvman.2020.111455.

[46] J. Huang, Molecular sieving effect of a novel hyper-cross-linked resin, Chem. Eng. J. 165 (1) (2010) 265-272. https://doi.org/10.1016/j.cej.2010.09.028.

[47] S. Ayyaru, Y. Ahn, Application of sulfonic acid group functionalized graphene oxide to improve hydrophilicity, permeability, and antifouling of PVDF nanocomposite ultrafiltration membranes, J. Membrane Sci. 525 (2017) 210-219. https://doi.org/10.1016/j.memsci.2016.10.048.

[48] M. Safarpour, V. Vatanpour, A. Khataee, Preparation and characterization of graphene

oxide/TiO_2 blended PES nanofiltration membrane with improved antifouling and separation performance, Desalination 393 (2016) 65-78. https://doi.org/10.1016/j.desal.2015.07.003.

[49] W. Hung, C. Tsou, M. De Guzman, Q. An, Y. Liu, Y. Zhang, C. Hu, K. Lee, J. Lai, Cross-linking with diamine monomers to prepare composite graphene oxide-framework membranes with varying *d*-spacing, Chem. Mater. 26 (9) (2014) 2983-2990. https://doi.org/10.1021/cm5007873.

[50] N. Meng, W. Zhao, E. Shamsaei, G. Wang, X. Zeng, X. Lin, T. Xu, H. Wang, X. Zhang, A low-pressure GO nanofiltration membrane crosslinked via ethylenediamine, J. Membrane Sci. 548 (2018) 363-371. https://doi.org/10.1016/j.memsci.2017.11.044.

[51] F. Kong, Q. Liu, L. Dong, T. Zhang, Y. Wei, J. Chen, Y. Wang, C. Guo, Rejection of pharmaceuticals by graphene oxide membranes:Role of crosslinker and rejection mechanism, J. Membrane Sci. 612 (2020) 118338. https://doi.org/10.1016/j.memsci.2020.118338.

[52] Y. Zhang, S. Zhang, T. Chung, Nanometric graphene oxide framework membranes with enhanced heavy metal removal via nanofiltration, Environ. Sci. Technol. 49 (16) (2015) 10235-10242. https://doi.org/10.1021/acs.est.5b02086.

Figure captions

Scheme 1 Schematic diagram of the dual regulation strategy of EMT and 1,4-Diaminobutane on GO membranes

Scheme 2 Preparation of NH2-GO/EMT composite membranes

Figure 1 (a) XRD pattern and (b) FT-IR spectrum of EMT-type zeolite

Figure 2 (a) SEM image and (b) TEM image of EMT-type zeolite nanosheet

Figure 3 Left: XRD patterns of samples; Right: peak fitting of XRD patterns of EMT, NH_2-GO/10EMT membrane (wet) and NH_2-GO/20EMT membrane (wet)

Figure 4 FT-IR spectra of (a) GO, (b) NH_2-GO/0EMT, (c) NH_2-GO/10EMT, and (d) NH_2-GO/20EMT

Figure 5 XPS elemental analysis of GO membrane and crosslinked GO membrane in the C1s region: (a) GO, (b) NH_2-GO/0EMT, (c) NH_2-GO/10EMT, and (d) NH_2-GO/20EMT

Figure 6 Cross-sectional SEM images of (a) GO membrane, (b) NH_2-GO/0EMT membrane, (c) NH_2-GO/10EMT membrane, and (d) NH_2-GO/20EMT membrane

Figure 7 SEM images with EDS of the surface for (a) GO membrane, (b) NH_2-GO/0EMT membrane, (c) NH_2-GO/10EMT membrane, and (d) NH_2-GO/20EMT membrane

Figure 8 Surface roughness of (a) GO membrane, (b) NH_2-GO/0EMT membrane, (c) NH_2-GO/10EMT membrane, and (d) NH_2-GO/20EMT membrane

Figure 9 Water contact angle of (a) GO membrane, (b) NH_2-GO/0EMT membrane, (c) NH_2-GO/10EMT membrane, and (d) NH_2-GO/20EMT membrane

Figure 10 Water flux of GO membrane and crosslinked GO membranes

Figure 11 MO separation performance of membranes: (a) water flux and (b) MO rejection

Figure 12 Dye rejection performance of NH_2-GO/10EMT membrane for different dyes

Figure 13 Anti-fouling performance of (a) GO, (b) NH_2-GO/0EMT and (c) NH_2-GO/10EMT membranes

Figure 14 Water flux recovery ratios and fouling resistance ratios of GO membrane, NH_2-GO/0EMT and NH_2-GO/10EMT membranes

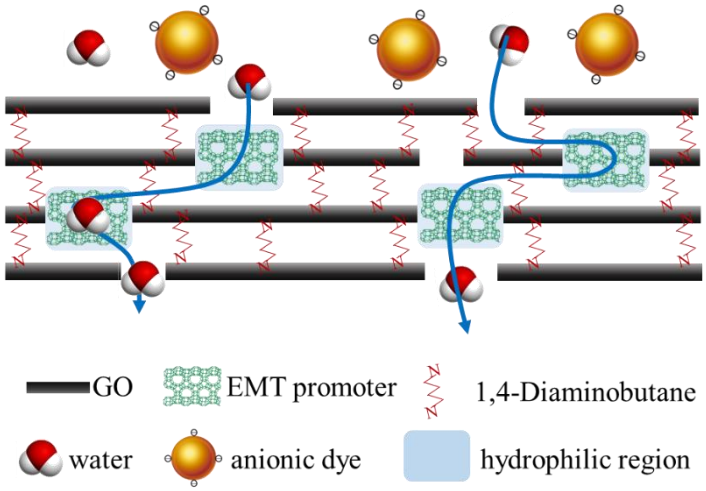

Scheme 1 Schematic diagram of the dual regulation strategy of EMT and 1,4-Diaminobutane on GO membranes

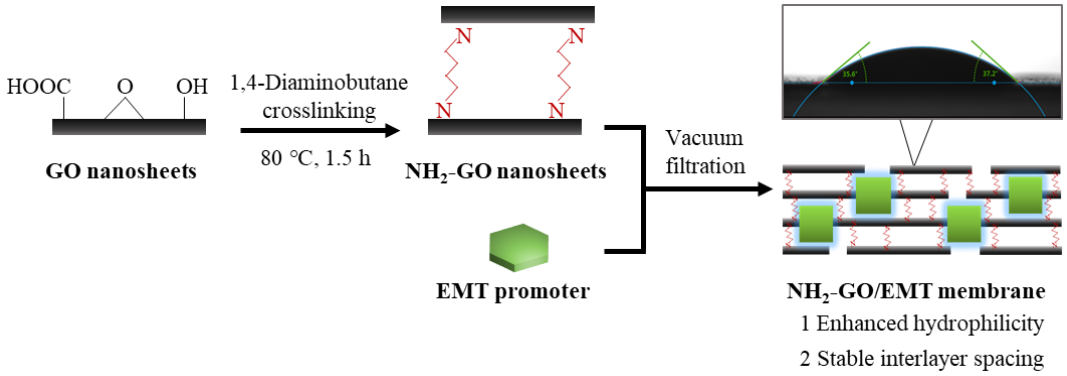

Scheme 2 Preparation of NH_2-GO/EMT composite membranes

1

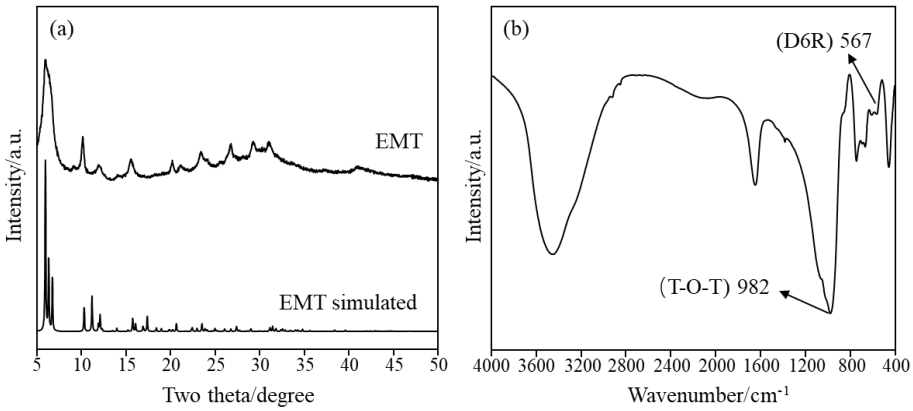

Figure 1 (a) XRD pattern and (b) FT-IR spectrum of EMT-type zeolite

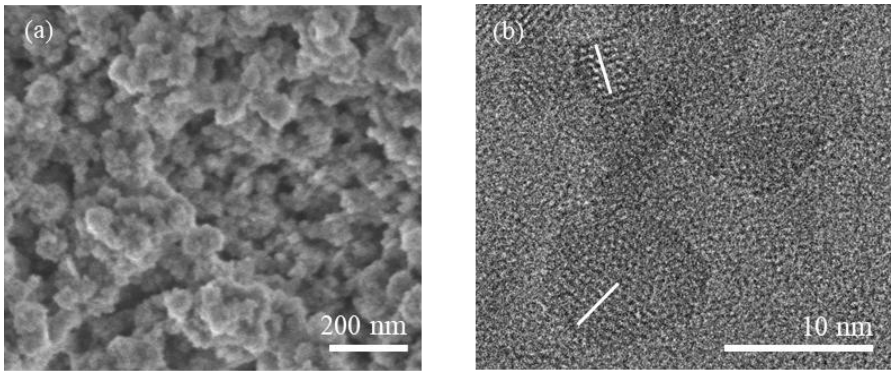

Figure 2 (a) SEM image and (b) TEM image of EMT-type zeolite nanosheet

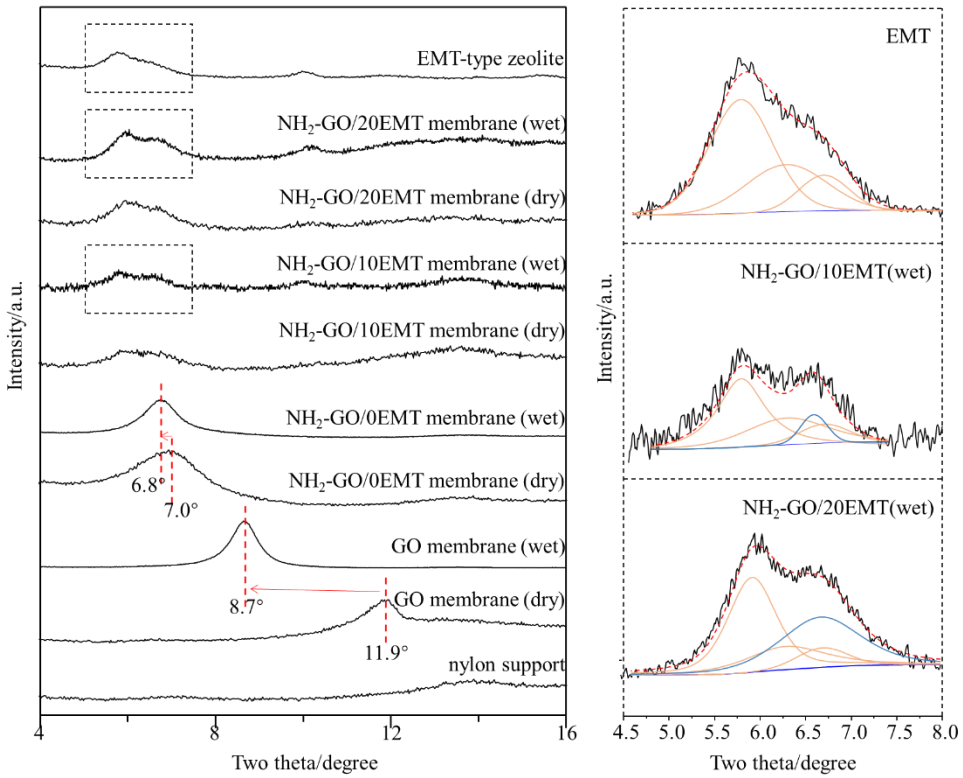

Figure 3 Left: XRD patterns of samples; Right: peak fitting of XRD patterns of EMT, NH_2-GO/10EMT membrane (wet) and NH_2-GO/20EMT membrane (wet)

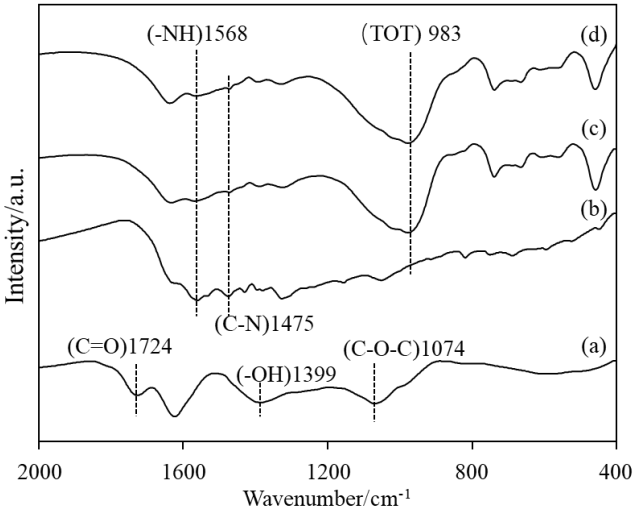

Figure 4 FT-IR spectra of (a) GO, (b) NH_2-GO/0EMT, (c) NH_2-GO/10EMT, and (d) NH_2-GO/20EMT

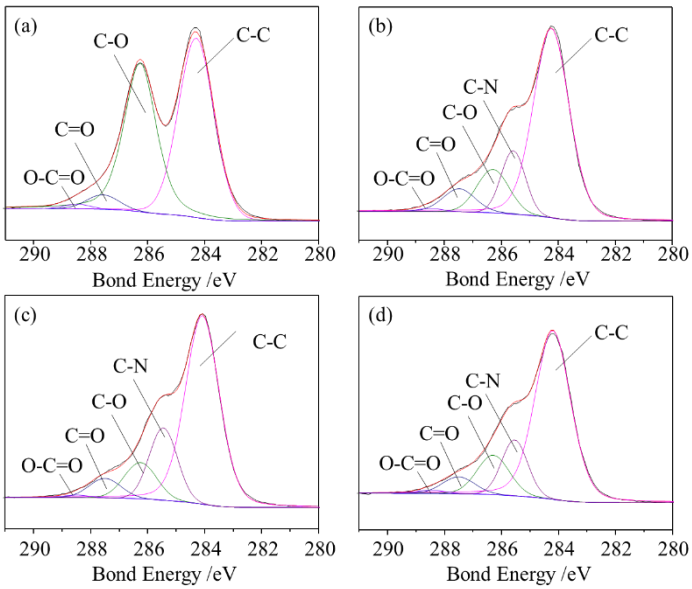

Figure 5 XPS elemental analysis of GO membrane and crosslinked GO membrane in the C1s region: (a) GO, (b) NH_2-GO/0EMT, (c) NH_2-GO/10EMT, and (d) NH_2-GO/20EMT

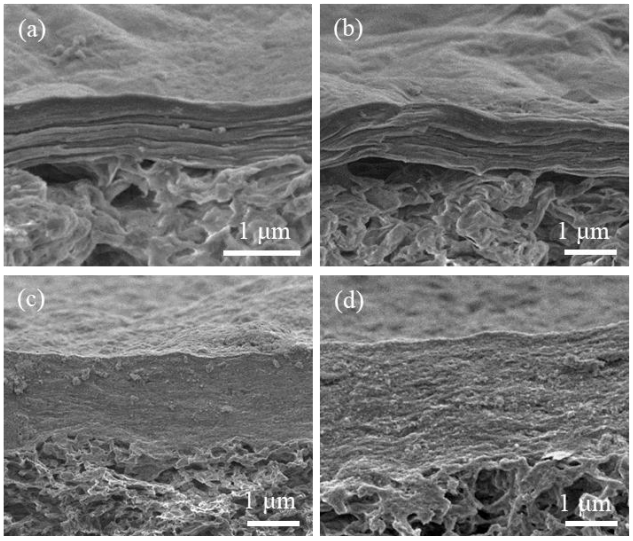

Figure 6 Cross-sectional SEM images of (a) GO membrane, (b) NH_2-GO/0EMT membrane, (c) NH_2-GO/10EMT membrane, and (d) NH_2-GO/20EMT membrane

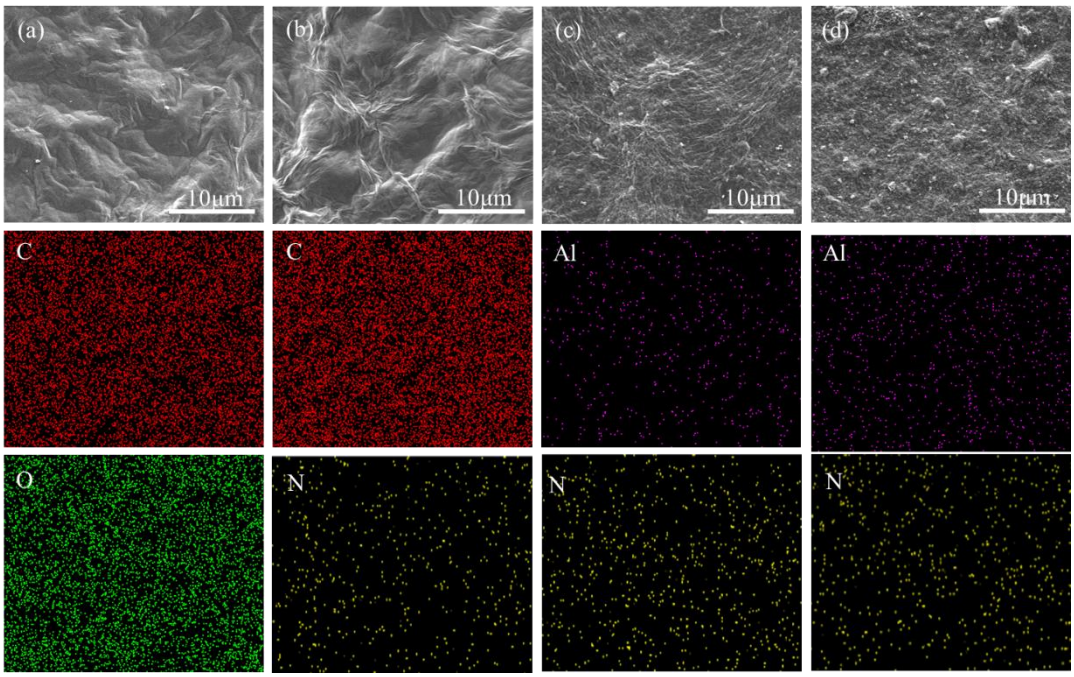

Figure 7 SEM images with EDS of the surface for (a) GO membrane, (b) NH_2-GO/0EMT membrane, (c) NH_2-GO/10EMT membrane, and (d) NH_2-GO/20EMT membrane

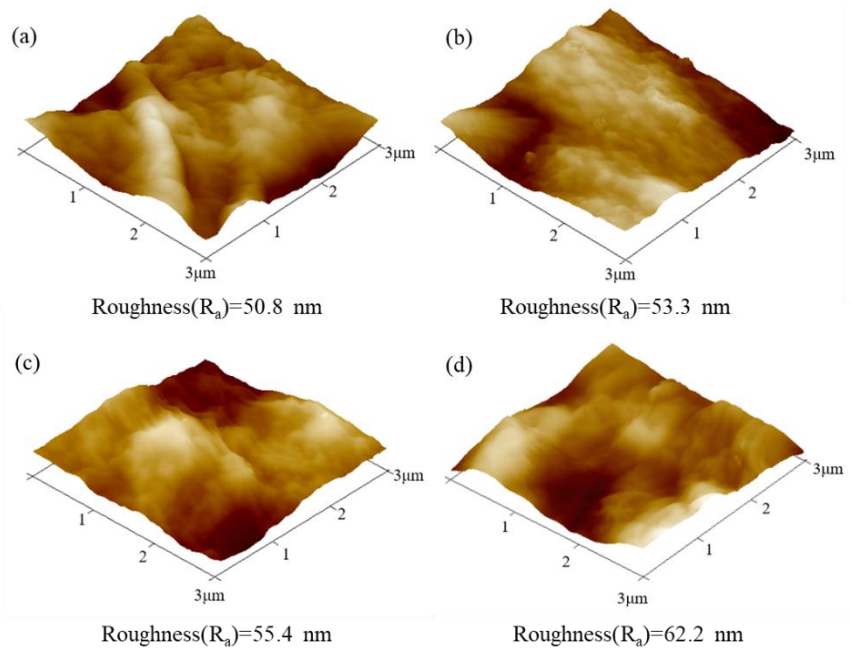

Figure 8 Surface roughness of (a) GO membrane, (b) NH_2-GO/0EMT membrane, (c) NH_2-GO/10EMT membrane, and (d) NH_2-GO/20EMT membrane

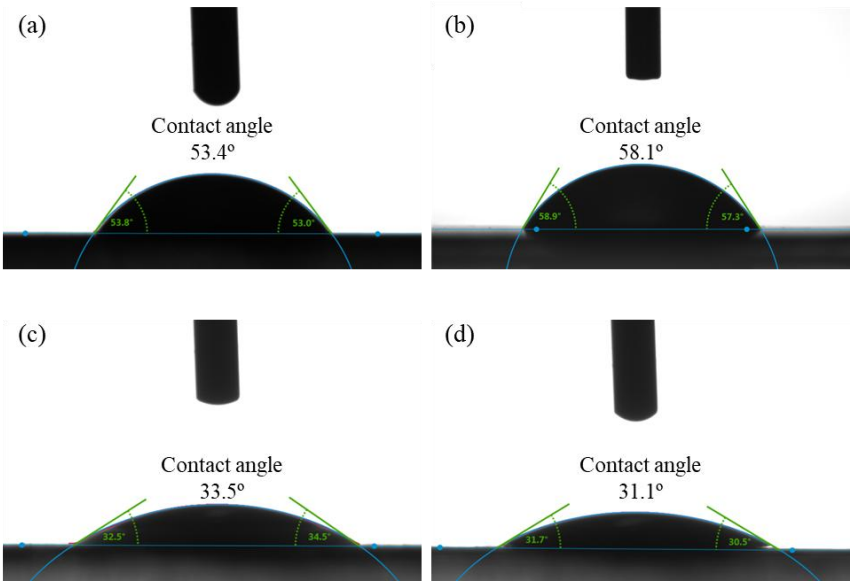

Figure 9 Water contact angle of (a) GO membrane, (b) NH_2-GO/0EMT membrane, (c) NH_2-GO/10EMT membrane, and (d) NH_2-GO/20EMT membrane

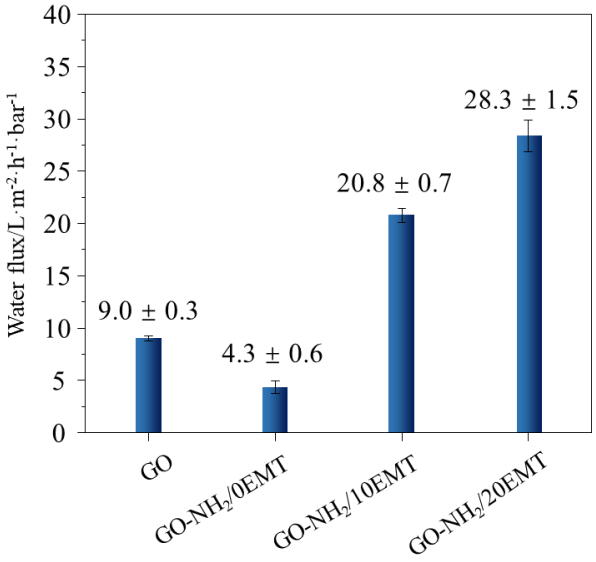

Figure 10 Water flux of GO membrane and crosslinked GO membranes

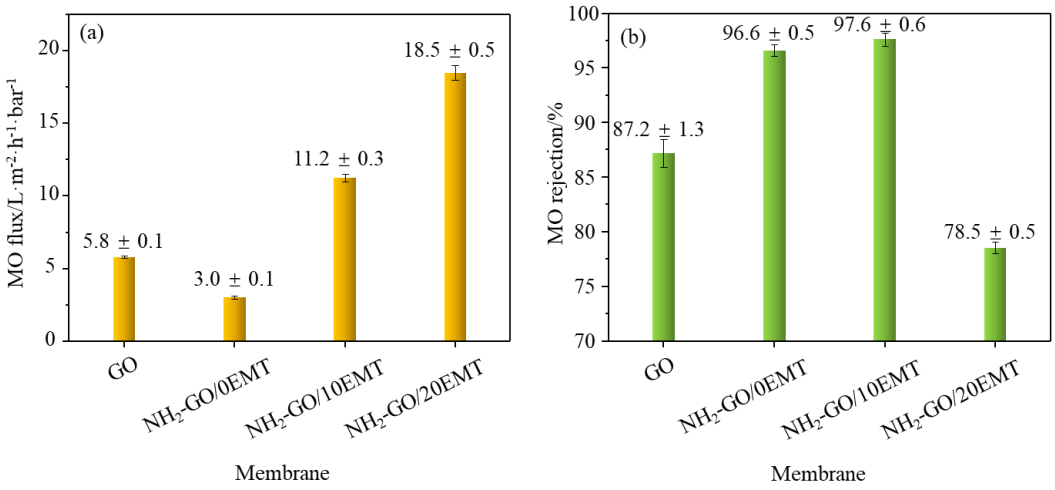

Figure 11 MO separation performance of membranes: (a) water flux and (b) MO rejection

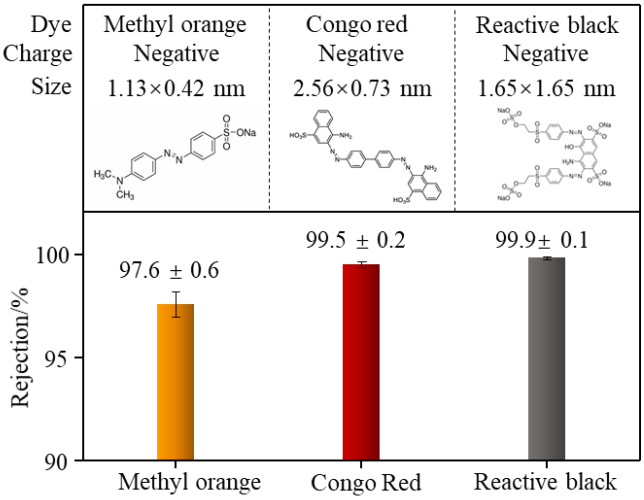

Figure 12 Dye rejection performance of NH_2-GO/10EMT membrane for different dyes

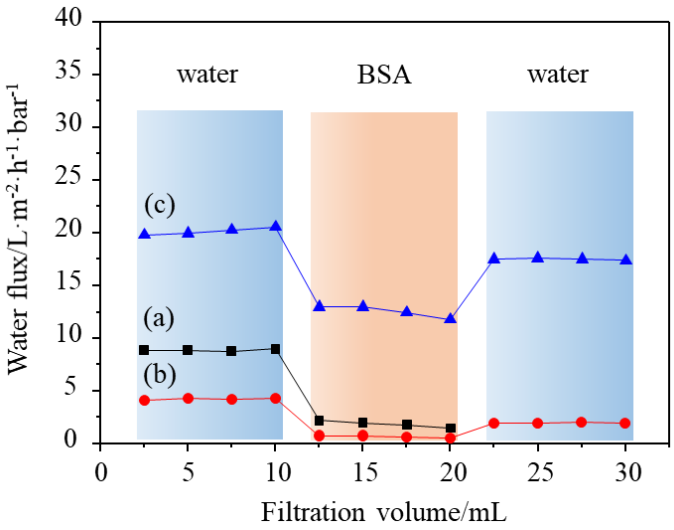

Figure 13 Anti-fouling performance of (a) GO, (b) NH_2-GO/0EMT and (c) NH_2-GO/10EMT membranes

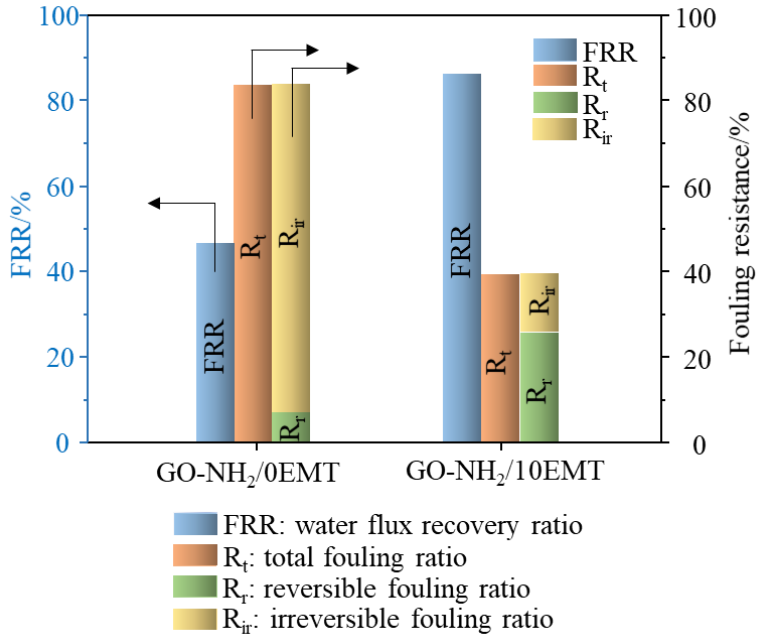

Figure 14 Water flux recovery ratios and fouling resistance ratios of GO membrane, NH_2-GO/0EMT and NH_2-GO/10EMT membranes